Structural Studies of Ammonia and Metallic Lithium−Ammonia Solutions

Helen Thompson,[†] Jonathan C. Wasse,[†] Neal T. Skipper,*,[†] Shusaku Hayama,[†,§]
Daniel T. Bowron,[‡] and Alan K. Soper[‡]

*Contribution from the Department of Physics and Astronomy, University College London,
Gower Street, London WC1E 6BT, United Kingdom, and Rutherford Appleton Laboratory,
Chilton, Didcot, Oxfordshire OX11 0QX, United Kingdom*

Received September 30, 2002 ; E-mail: n.skipper@ucl.ac.uk

Abstract: The technique of hydrogen/deuterium isotopic substitution has been used to extract detailed information concerning the solvent structure in pure ammonia and metallic lithium−ammonia solutions. In pure ammonia we find evidence for approximately 2.0 hydrogen bonds around each central nitrogen atom, with an average N−H distance of 2.4 Å. On addition of alkali metal, we observe directly significant disruption of this hydrogen bonding. At 8 mol % metal there remains only around 0.7 hydrogen bond per nitrogen atom. This value decreases to 0.0 for the saturated solution of 21 mol % metal, as all ammonia molecules have then become incorporated into the tetrahedral first solvation spheres of the lithium cations. In conjunction with a classical three-dimensional computer modeling technique, we are now able to identify a well-defined second cationic solvation shell. In this secondary shell the nitrogen atoms tend to reside above the faces and edges of the primary tetrahedral shell. Furthermore, the computer-generated models reveal that on addition of alkali metal the solvent molecules form voids of approximate radius 2.5−3.0 Å. Our data therefore provide new insight into the structure of the polaronic cavities and tunnels, which have been theoretically predicted for lithium−ammonia solutions.

I. Introduction

Interest in the microscopic structure of liquid ammonia arises mainly from the propensity of the NH₃ molecules to form hydrogen bonds, and the ability to act as a stable solvent for a variety of chemically reactive species. For example, liquid ammonia is used as a catalyst for many common organic reactions. It is also able to dissolve many metals, and thereby release the valence electrons into solution.

The lowest energy configuration of the $(NH_3)_2$ dimer is an off-linear hydrogen bond,[1] with a dissociation energy of approximately 12 kJ mol⁻¹ and an N−N distance of 3.26 Å. The dimer energy surface, however, is uncommonly flat near equilibrium. This, coupled with the fact that the ammonia molecule has only one lone pair available to accept a hydrogen bond, leads one to expect quite weak association in the liquid state. In fact, the internal energy of liquid ammonia is around 21 kJ mol⁻¹,[2,3] approximately half the value for bulk water.[4] Indeed, previous neutron and X-ray diffraction experiments and computer simulations have pointed to quite weak hydrogen bonding in liquid ammonia, without the formation of an extended network.[2−6]

Dissolution of alkali metal into liquid ammonia produces intensely colored "metal solutions", in which dissociation of the valence electrons from the alkali-metal ions gives rise to a rich variety of ionic and electronic species,[7] for example, solvated cations, solvated electrons, spin-paired electrons (bipolarons), contact-ion pairs, ion triples, and dielectron pairs.[8−11] Furthermore, at around 4 mol % metal (MPM), the solutions pass through a metal−nonmetal transition.[7] This yields brilliant bronze-colored solutions of remarkably low density, in which the strongly reducing electrons are apparently fully delocalized.

Much interest now lies in the structure of these metallic solutions, particularly the nature of the solvent−solvent interactions and their involvement in the metal−nonmetal transition. Key questions to be answered include the impact of added metal on the hydrogen bonding, and the way in which the metal−ammonia solution is then able to accommodate the cations and excess electrons. With respect to the solvated excess electrons, one is looking in particular for evidence that the solvent is able to form cavities, channels, or low-density regions through which these electrons might percolate.[7] Such polaronic structures have been predicted theoretically.[3,12,13]

[†] University College London.

[‡] Rutherford Appleton Laboratory.

[§] Present address: Department of Physics, King's College London, Strand, London WC2R 2LS.

(1) Loeser, J. G.; Schmuttenmaer, C. A.; Cohen, R. C.; Elrod, M. J.; Steyert, D. W.; Saykally, R. J.; Bumgarner, R. E.; Blake, G. A. *J. Chem. Phys.* **1992**, *97*, 4727.
(2) Jorgensen, W. L.; Ibrahim, M. *J. Am. Chem. Soc.* **1980**, *102*, 3309.
(3) Impey, R. W.; Sprik, M.; Klein, M. L. *J. Am. Chem. Soc.* **1987**, *109*, 5900.
(4) Goldman, N.; Fellers, R. S.; Brown, M. G.; Braly, L. B.; Keoshin, C. J.; Leforestier, C.; Saykally, R. J. *J. Chem. Phys.* **2002**, *116*, 10148.

(5) Narten, A. H. *J. Chem. Phys.* **1977**, *66*, 3117.
(6) Ricci, M. A.; Nardone, M.; Ricci, F. P.; Andreani, C.; Soper, A. K. *J. Chem. Phys.* **1995**, *102*, 7650.
(7) Thompson, J. C. *Electrons in Liquid Ammonia*; Clarendon: Oxford, 1976.
(8) Holton, D.; Edwards, P. P. *Chem. Br.* **1985**, 1007.
(9) Edwards, P. P. *Phys. Chem. Liq.* **1981**, *10*, 189.
(10) Edwards, P. P. *Adv. Inorg. Chem. Radiochem.* **1982**, *25*, 135.
(11) Edwards, P. P. *J. Phys. Chem.* **1984**, *88*, 3772.
(12) Deng, Z.; Martyna, G. J.; Klein, M. L. *Phys. Rev. Lett.* **1993**, *71*, 267.

In this paper the technique of hydrogen/deuterium isotopic substitution in neutron diffraction has been used to investigate the structure of the pure ammonia solvent, and metallic lithium−ammonia solutions at 8 mol % metal (NH_3:Li = 92:8) and 21 mol % metal (NH_3:Li = 79:21). This technique gives us unparalleled insight into the hydrogen-bonding structure in these systems, which complements recent computer simulation[3,12,13] and X-ray[5,16] and neutron diffraction studies.[14,15,17,18]

By focusing here on the H-centered correlations, we are able to show directly that the hydrogen bonding is severely disrupted by addition of metal, and is in fact completely absent at saturation. In addition, we show that second-shell N−H and H−H distances *increase* with metal concentration, due to a decrease in overall density as the number of excess electrons increases. In contrast to this, our data exhibit a *decrease* in the nearest-neighbor N−N peak position, plus a narrowing of the peak width, as one moves from pure ammonia to the metallic phase. This is due to the strong tetrahedral solvation of the lithium cations in the metallic phase.[17,18] A three-dimensional modeling technique[19] has then been applied to our neutron diffraction data. The resulting model enables us to confirm the presence, and orientation, of a second cationic solvation shell. In addition, it enables us to tackle the question of how polaronic cavities are formed within the solvent, and the way in which percolation channels may then arise in the metallic lithium−ammonia solutions.[12]

II. Theoretical Background

Hydrogen/deuterium isotopic substitution[20] takes full advantage of the very large difference in neutron scattering lengths between hydrogen ($b_H = -3.74$ fm) and deuterium ($b_D = 6.67$ fm). By performing experiments on three samples, which are identical in every respect apart from the isotopic composition of the hydrogen atoms, it is possible to extract the three partial structure factors $S_{HH}(k)$, $S_{XH}(k)$, and $S_{XX}(k)$, where the subscript H refers to substituted hydrogen atoms and X refers to any nonsubstituted atom.

After corrections, the quantity that can be extracted from a single neutron diffraction experiment is the total structure factor, which can be expressed as

$$F(k) = \sum_{\alpha\beta} c_\alpha c_\beta b_\alpha b_\beta [S_{\alpha\beta}(k) - 1] \qquad (1)$$

where c_α is the atomic fraction of species α, b_α is the neutron scattering length of atom α, $k = 4\pi(\sin\theta)/\lambda$ (i.e., the magnitude of the momentum change vector of the scattered neutrons), and $S_{\alpha\beta}(k)$ is the Faber−Ziman partial structure factor involving atoms α and β only. In the current context, this total structure factor can be written as a sum of three composite partial structure

factors:

$$F(k) = c_X^2 b_X^2 [S_{XX}(k) - 1] + 2c_X c_H b_X b_H [S_{XH}(k) - 1] + c_H^2 b_H^2 [S_{HH}(k) - 1] \quad (2)$$

where the composite coherent scattering length b_X and atomic concentration c_X are defined as

$$b_X = \sum_{\alpha \neq H} c_\alpha b_\alpha / c_X, \quad c_X = \sum_{\alpha \neq H} c_\alpha, \quad c_H = 1 - c_X \qquad (3)$$

Specifically, the $S_{HH}(k)$ partial structure factor is calculated from

$$S_{HH}(k) - 1 = \{xF_H(k) + (1 - x)F_D(k) - F_{HD}(k)\}/ \{c_H^2[xb_H^2 + (1 - x)b_D^2 - b_{HD}^2]\} \quad (4)$$

where the subscripts H, D, and HD refer to the total structure factors for the protonated, deuterated, and mixture samples, respectively, and x is the fraction of protonated ammonia in the mixture sample. Then

$$b_{HD} = xb_H + (1 - x)b_D \qquad (5)$$

Similarly, the XH and XX composite partial structure factors are calculated via the following relations:

$$S_{XH}(k) - 1 = \{F_H(k) - F_D(k) + c_H^2(b_D^2 - b_H^2)[S_{HH}(k) - 1]\}/\{2c_H c_X b_X (b_H - b_D)\} \quad (6)$$

$$S_{XX}(k) - 1 = \{F_H(k) - 2c_H c_X b_H b_X [S_{XH}(k) - 1] - c_H^2 b_H^2 [S_{HH}(k) - 1]\}/c_X^2 b_X^2 \quad (7)$$

The weighting coefficients of the contributions to the X−H and X−X partial functions are shown in Table 1, and the composite partial structure factors are then given by

$$S_{XH}(k) - 1 = \sum_{\alpha \neq H} c_\alpha b_\alpha [S_{\alpha H}(k) - 1]/c_X b_X \qquad (8)$$

$$S_{XX}(k) - 1 = \sum_{\alpha \neq H, \beta \neq H} c_\alpha b_\alpha c_\beta b_\beta [S_{\alpha\beta}(k) - 1]/c_X^2 b_X^2 \quad (9)$$

A Fourier transform yields the partial pair correlation function, $g_{\alpha\beta}(r)$, given by

$$g_{\alpha\beta}(r) - 1 = \int_0^\infty \{k[S_{\alpha\beta}(k) - 1]\sin(kr)\,dk\}/(2\pi^2 n_0 r) \quad (10)$$

where k is the scattering vector, r is a position in real space, and n_0 is the atomic number density of the sample. The resulting partial pair correlation function provides a wealth of information concerning both intra- and intermolecular atom−atom distances and coordination numbers. The average number of atoms of type β surrounding an atom of type α, between radii r_1 and r_2, is calculated from

$$\bar{n}_\beta^\alpha = 4\pi n_0 c_\beta \int_{r_1}^{r_2} r^2 g_{\alpha\beta}(r)\,dr \qquad (11)$$

where n_0 is again the average atomic number density of the sample.

III. Experimental and Analysis Procedures

Neutron diffraction data were collected at the Small Angle Neutron Diffractometer for Liquids and Amorphous Samples (SANDALS) at the ISIS pulsed neutron source, Rutherford Appleton Laboratory, U.K.

(13) Diraison, M.; Martyna, G. J.; Tuckerman, M. E. *J. Chem. Phys.* **1999**, *111*, 1096.
(14) Hayama, S.; Wasse, J. C.; Skipper, N. T. *J. Phys. Chem. B* **2001**, *106*.
(15) Hayama, S.; Wasse, J. C.; Skipper, N. T.; Walters, J. K. *Mol. Phys.* **2001**, *99*, 779.
(16) Hayama, S.; Wasse, J. C.; Skipper, N. T.; Thompson, H. *J. Chem. Phys.* **2002**, *116*, 2991.
(17) Wasse, J. C.; Hayama, S.; Skipper, N. T.; Fischer, H. E. *Phys. Rev. B* **2000**, *61*, 11993.
(18) Wasse, J. C.; Hayama, S.; Skipper, N. T.; Benmore, C. J.; Soper, A. K. *J. Chem. Phys.* **2000**, *112*, 7147.
(19) McGreevy, R. L.; Howe, M. A. *Annu. Rev. Mater. Sci.* **1992**, *22*, 217.
(20) Bowron, D. T.; Soper, A. K.; Finney, J. L. *J. Chem. Phys.* **2001**, *114*, 6203.

Table 1. Weighting Coefficients for the Contributions to the X—X, X—H, and H—H Terms for the 0, 8, and 21 MPM Solutions

	0 MPM	8 MPM	21 MPM
H—H partial			
H—H	1.000	1.000	1.000
X—H partial			
N—H	1.000	1.018	1.057
Li—H		−0.018	−0.057
X—X partial			
N—N	1.000	1.036	1.117
N—Li		−0.036	−0.121
Li—Li		0.0003	0.0033

This instrument is optimized for the measurement of the structure of liquid and amorphous samples, and in particular for hydrogen/deuterium substitution.[20]
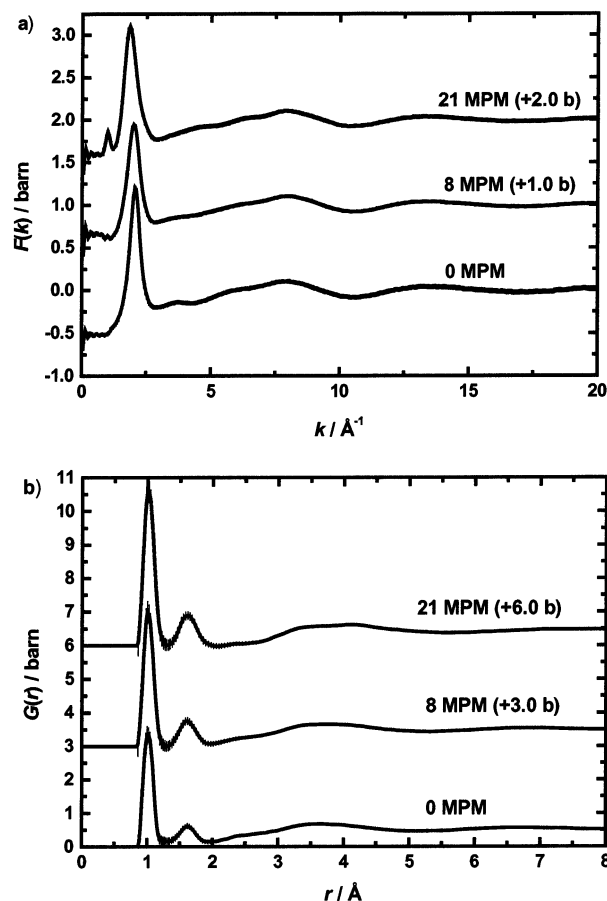
To prepare the metal solutions, an ingot of lithium was mechanically cleaned, and then weighed in a dry argon atmosphere glovebox (O_2 and H_2O less than 10 ppm). This freshly cut piece of lithium was loaded into a highly polished flat-plate null coherent scattering titanium/zirconium cell, with 1 mm sample and wall thicknesses. This geometry minimizes multiple neutron scattering and absorption. The sample cell was then sealed, removed from the glovebox, and attached to a closed cycle refrigerator on the beam line. Prior to in situ condensation of ammonia, the cell was connected to a purpose-built stainless steel gas rig via a 1/8 in. capillary, and was evacuated to a pressure of less than 10^{-5} mbar. A known volume of ammonia gas was condensed directly onto the lithium metal held at 230 K, to achieve the required concentration of metal in solution. The temperature of 230 K was chosen to be below the boiling point of ammonia, and to avoid the region of phase separation occurring at ∼210 K.[7]

For each sample, a series of about eight neutron diffraction data sets were collected over a total of 10 h. During this time, the stability of the solutions was monitored by checking the consistency of the raw data, and by measuring the gas pressure over the solution. No significant change in gas pressure was recorded, and we therefore conclude that there was no significant decomposition of solution to the amide (Li—NH_2) plus hydrogen gas.

Data were collected at two concentrations for the metallic solutions: 8 and 21 MPM. At each concentration we measured three isotopically distinct samples: Li—ND_3, Li—NH_3, and a 50:50 mixture of Li—ND_3 and Li—NH_3 (50:50 being chosen here to maximize the scattering differences between the samples). Diffraction data were also collected for pure liquid ammonia, the three samples here being ND_3, NH_3, and a 33:67 mixture of ND_3 and NH_3 (a so-called "null-scattering" mixture). For data correction and calibration, scattering data were also collected from the empty instrument (with and without the empty sample cell), and an incoherent scattering vanadium standard slab of thickness 3.48(2) mm.

Background, multiple scattering, absorption, and normalization analysis procedures were implemented by the ATLAS[21,22] suite of programs, to give the differential scattering cross-section for each isotopically distinct sample. Polynomials, representing the self-scattering and inelastic scattering, were then subtracted from the normalized differential cross-sections to yield the total static structure factors.

The three target composite partial structure factors X—X, X—H, and H—H were formed using eqs 4—7. At this stage it was deemed necessary to perform a further semiempirical inelastic scattering correction to the low-Q region of these partial structure factors, because of the large number of hydrogen atoms present in our samples.[20] The

(21) Soper, A. K.; Howells, W. S.; Hannon, A. C. *Atlas-Analysis of Time-of-flight Diffraction data from Liquid and Amorphous Samples*; Rutherford Appleton Laboratory Report RAL-89-046; Rutherford Appleton Laboratory: Oxfordshire, U.K., 1989.
(22) Soper, A. K. In *Neutron Scattering Data Analysis 1990*; Johnson, M. W., Ed.; IOP Conference Series Number 107; IOP Publishing: Bristol, U.K., 1990; pp 57—67.

Figure 1. (a) Total structure factors (error bars) and MIN fit (solid line) and (b) total radial distribution functions for the deuterated samples.

efficacy of these procedures was verified by checking the self-consistency of the composite partial structure factors and their Fourier back-transforms.

A minimum noise transform was used to produce the radial distribution functions presented here.[22,23] This method of Fourier transformation is an iterative technique, which attempts to generate pair correlation functions, $g_{\alpha\beta}(r)$, which are as smooth as possible while still consistent with the data. In this way we are able to focus on real features, and not, for example, those that might be caused by truncation of the structure factor and/or noise within the data.

Finally, a so-called reverse Monte Carlo (RMC)[19] molecular modeling technique was used to generate a 3-dimensional ensemble consistent with the experimental data and known structural constraints, for example, intramolecular atom—atom distances, the geometry of the ammonia molecule, and the tetrahedral solvation of lithium cations.[17] The data sets used for the RMC modeling comprised the total static structure factors for the fully deuterated, fully protonated, and mixed samples. In each simulation, the minimum number of atoms used was 3000. The atomic density was set to the experimental value and a cubic box side of approximately 35 Å calculated accordingly. This method allowed us to probe the angular orientations of the solvent molecules, relative to each other and the lithium cation (the latter using a predefined axis for the Li—$(NH_3)_4$ tetrahedron). In addition, the final model reveals for the first time the structure and concentration of the polaronic cavities, which may accommodate the excess electrons.
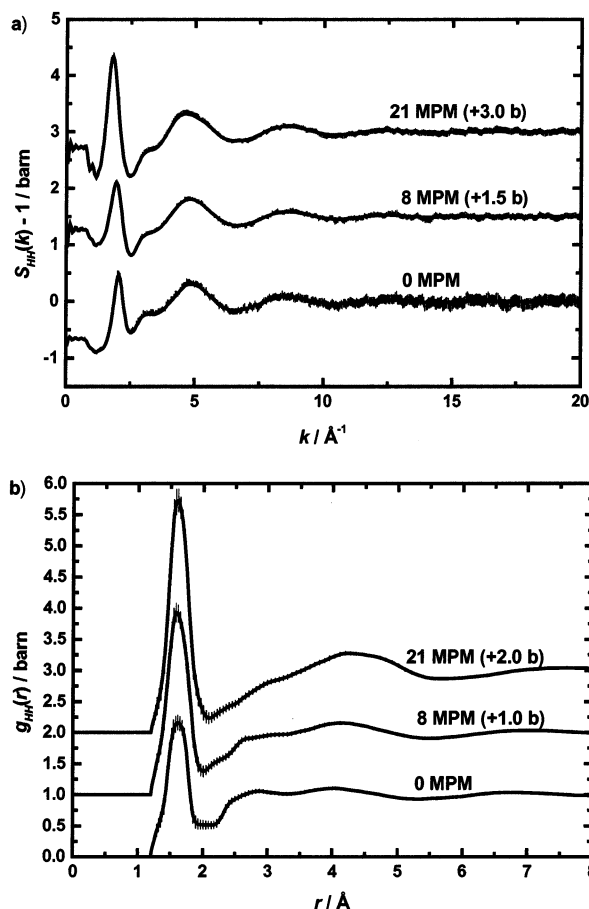
IV. Results and Discussion

We have studied liquid ammonia and metallic solutions of lithium in ammonia at 8 and 21 MPM using hydrogen/deuterium

(23) Soper, A. K.; Andreani, C.; Nardone, M. *Phys. Rev. E* **1993**, *47*, 2598.

Figure 2. (a) H−H partial structure factor (error bars) and MIN fit (solid line) and (b) H−H partial radial distribution function.
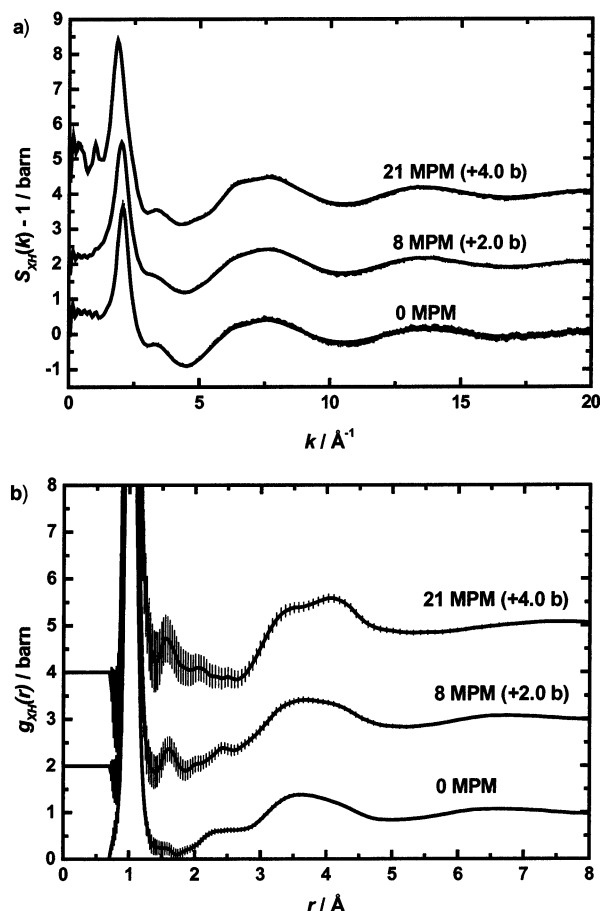

Figure 3. (a) X−H partial structure factor (error bars) and MIN fit (solid line) and (b) X−H partial radial distribution function.

isotopic substitution. Our experiments therefore provide us with total static structure factors (eq 2), and the partial static structure factors and pair correlation functions for X−X, X−H, and H−H correlations (eqs 4, 6, 7, and 10).

The measured total structure factors, the minimum noise fit, and the total pair correlation functions for 0, 8, and 21 MPM lithium−ammonia solutions are presented in Figure 1. The minimum noise fit shows excellent agreement with the measured data, and therefore gives us confidence in the data analysis techniques used.[20] Upon addition of lithium metal to ammonia, a decrease in the position of the principal peak in $F(k)$ is observed, from 2.07(2) Å^{-1} in liquid ammonia, to 2.01(2) and 1.85(2) Å^{-1} in 8 and 21 MPM solutions, respectively.[6,17,18] This shift is consistent with the reduction in solution density with metal concentration, as the solvent expands to accommodate the excess electrons as they are dissociated from the lithium atoms.[7] For the saturated (21 MPM) solution, the presence of a prepeak at ∼1 Å^{-1} indicates intermediate-range ordering in the solution. This feature is associated with correlations between solvated cations,[17] and is discussed in detail in this section.

Figures 2−4 show the composite partial structure factors, together with the corresponding composite partial pair correlation functions, for H−H, X−H, and X−X. From these functions we note first that all intramolecular distances within the ammonia molecules are unaffected by the presence of the lithium cations and excess electrons. We then observe that, in accordance with the total structure factors, the principal peak position in all three of the partial structure factors decreases

with metal content. This effect reflects the overall reduction in solution density, and leads to corresponding peak shifts in the high-r region of the partial radial distribution functions.

To determine the nearest-neighbor distances and coordination numbers, each of the partial pair correlation functions has been plotted as $r^2g(r)$, and a Gaussian curve fitting procedure has been applied, as shown in Figures 5−7 and Tables 2−4. This analysis is able to separate the quite broad features typical in liquid structures, and therefore provides the basis for quantitative discussion of the local structure in our solutions, as follows.

A. Hydrogen Bonding and Solvent Structure. In the context of hydrogen bonding, the key functions are the X−H partial structure factors and radial distributions (eqs 6 and 10). These functions are shown in Figures 3 and 6, and contain direct information about the intermolecular N−H correlations. It is immediately clear that the size of the shoulder at ∼2.4 Å due to N−H hydrogen bonding decreases with metal concentration. This shoulder merges into a broad peak at around 3.6 Å, which we assign to non-hydrogen-bonded (van der Waals) contacts. Gaussian fitting to $r^2g(r)$ in this region (Table 3) shows that in the pure solvent the number of hydrogen bonds per nitrogen atom is 2.1 ± 0.5, in good agreement with previous neutron and computer simulation studies. Note here that in solid ammonia there are 3.0 hydrogen bonds per molecule.[24−26]

(24) Reed, J. W.; Harris, P. M. *J. Chem. Phys.* **1961**, *35*, 1730.
(25) Hewat, A. W.; Riekel, C. *Acta Crystallogr.* **1979**, *A35*, 569.
(26) Olovsson, I.; Templeton, D. H. *Acta Crystallogr.* **1959**, *12*, 832.
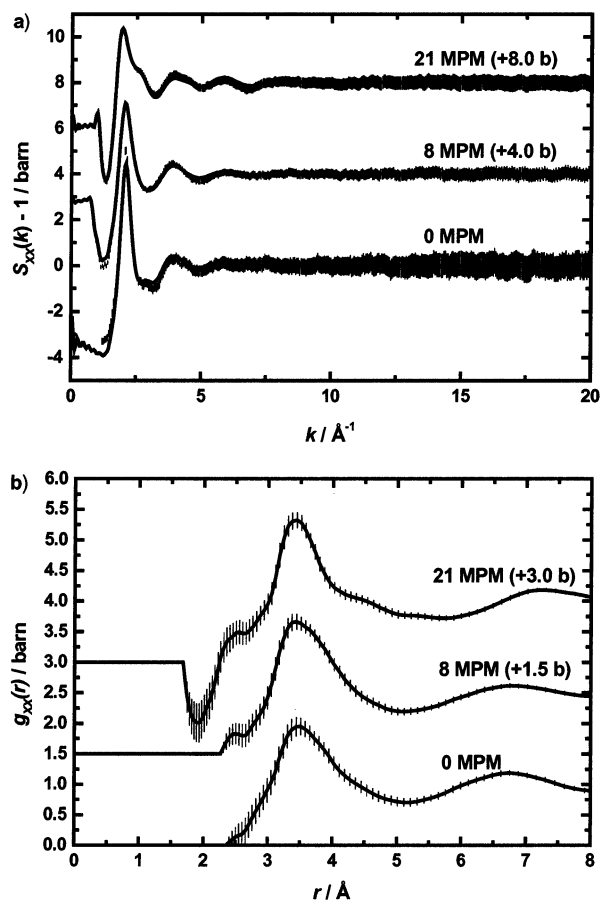
Figure 4. (a) X—X partial structure factor (error bars) and MIN fit (solid line) and (b) X—X partial radial distribution function.

Addition of lithium metal causes a large decrease in the number of hydrogen bonds per nitrogen atom, to only 0.7 bond per nitrogen atom for the 8 MPM solution. Furthermore, for the 21 MPM saturated solution, the hydrogen-bonded N—H shoulder disappears altogether as all the remaining ammonia molecules become involved in the solvation shell of the lithium cation. This disruption to the hydrogen-bonded network coincides with the formation of the extended polaronic electron cavities that leads to the metallic state, and the uncommonly low density at saturation. We discuss these issues in subsection C.
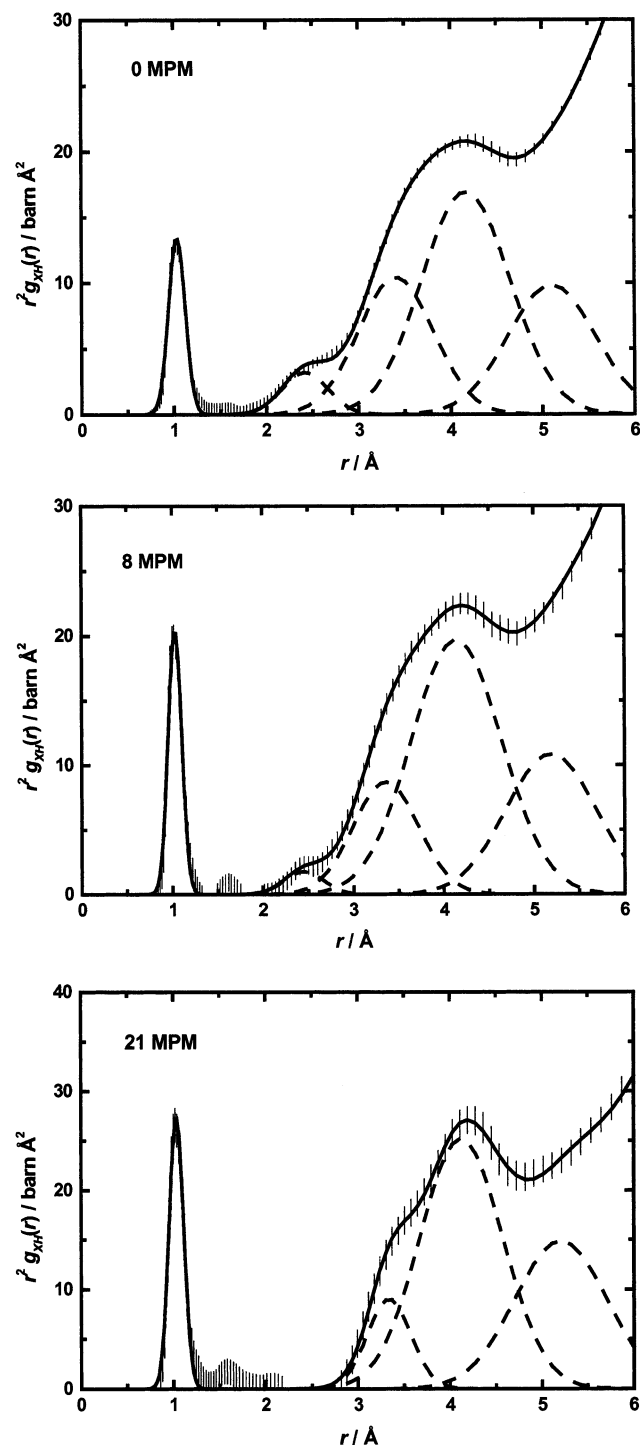
The H—H partial pair correlation function shown in Figure 2 confirms our conclusions on the disruption of hydrogen bonding. At 0 MPM (pure ammonia), a large feature is evident at ~2.9 Å. This is equivalent to the distance between two hydrogen atoms on two adjacent hydrogen-bonded molecules[6] (taking the hydrogen-bonding angle to be 107°). Again the $r^2g_{HH}(r)$ function has been fitted with Gaussians (Figure 5), and as may be expected, the estimated coordination number of nearest-neighbor H—H correlations decreases rapidly, from ~7.5 atoms in pure ammonia, to 5 atoms in 8 MPM solution, to only 3 atoms for the saturated solution.

We now move to the X—X correlations, which contain a strong contribution due to N—N interactions. Here we note that the first N—N peak position shifts *inward* in real space, from 3.48(2) Å in pure ammonia to 3.44(2) Å in 8 MPM solution and 3.42(2) in the 21 MPM solution. At first this trend may seem counterintuitive, especially when one remembers the
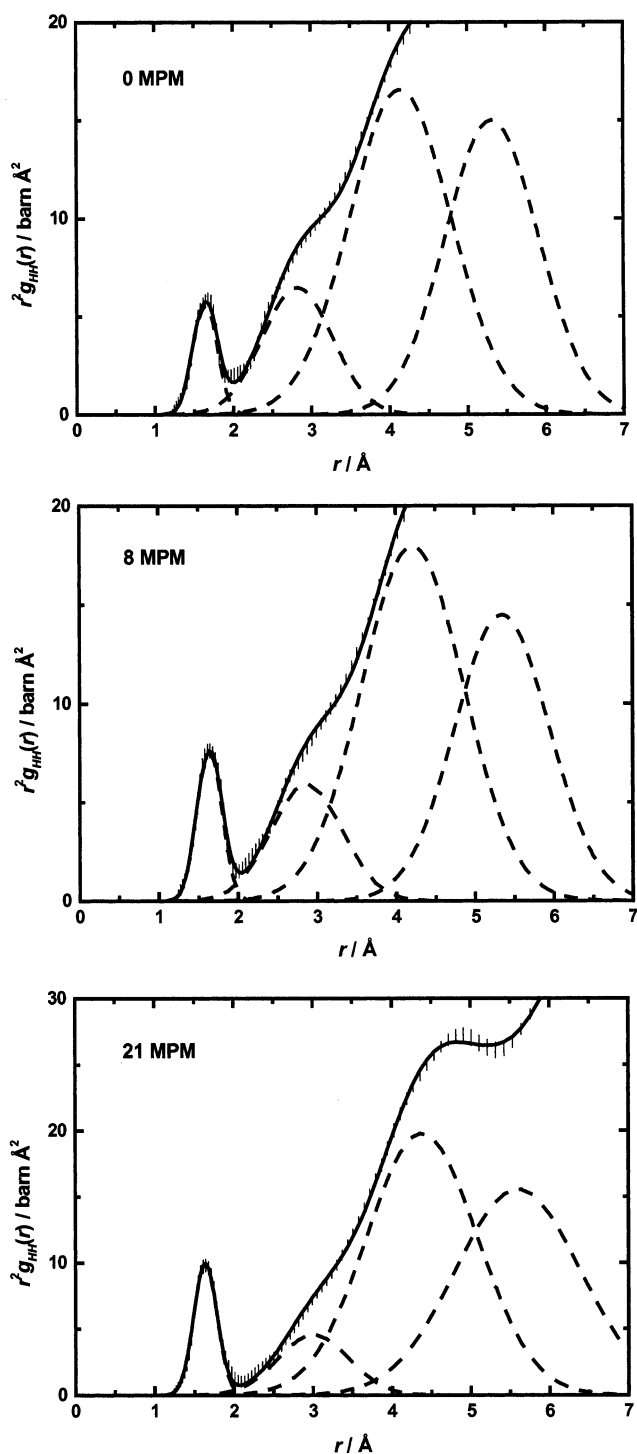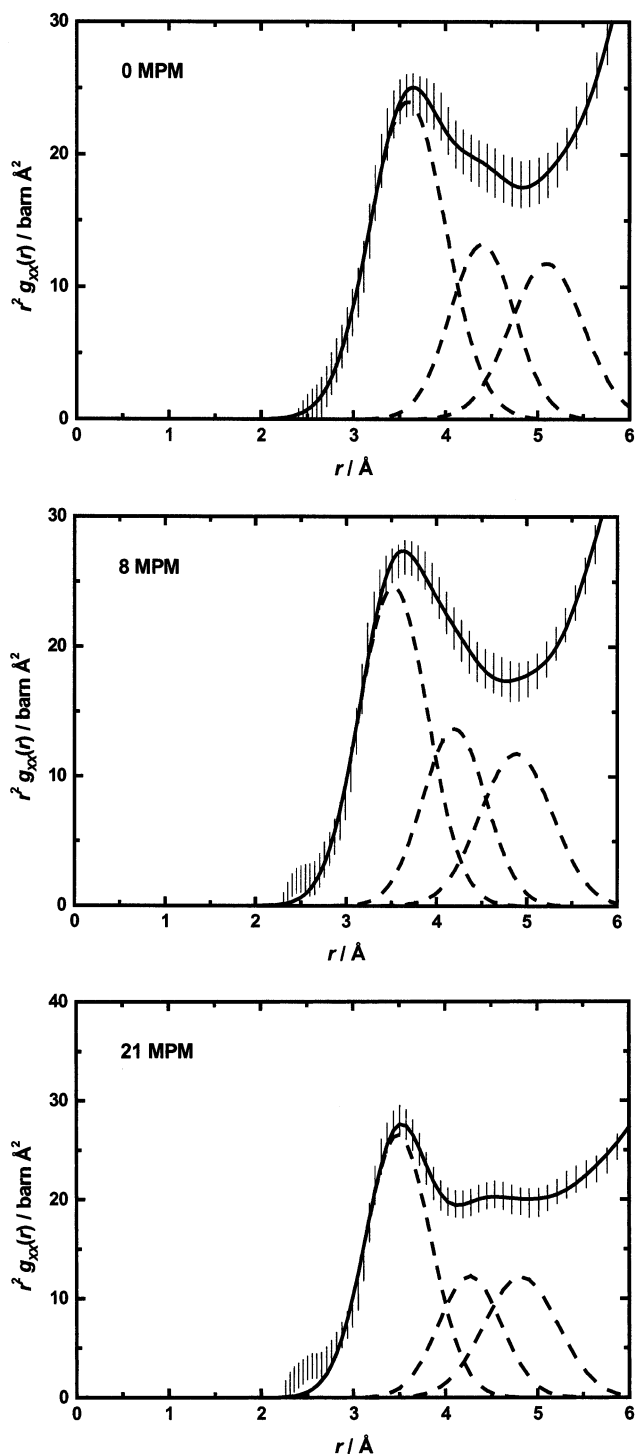

Figure 5. Gaussian fits to $r^2g_{HH}(r)$. The error bars show the measured data, the solid lines the total Gaussian fit and the individual Gaussian peaks.

decreasing density as metal concentration increases. However, this shift in the values of nearest-neighbor N—N distances reflects the "tighter binding" between the ammonia molecules involved in the cationic solvation spheres than that existing between the ammonia molecules in the pure solvent. The concomitant narrowing of the nearest-neighbor N—N peak width is consistent with this interpretation. As one would hope, our nearest-neighbor N—N peak positions are in extremely close agreement with recent X-ray work,[16] as are the N—N first-shell coordination numbers.

Figure 6. Gaussian fits to $r^2 g_{XH}(r)$. The error bars show the measured data, the solid lines the total Gaussian fit and the individual Gaussian peaks.

Figure 7. Gaussian fits to $r^2 g_{XX}(r)$. The error bars show the measured data, the solid lines the total Gaussian fits and the individual Gaussian peaks.

Our first peak in the X−X partial pair correlation function in pure ammonia, relating to first-shell N−N correlations, is asymmetric on the high-r side.[5,6] The general shape of the N−N peak presented here, although not split, is consistent with Narten's measured N−N distances of 3.73 and 3.40 Å,[5] which show some of the 12 neighboring ammonia molecules to be in van der Waals contact and some to be hydrogen-bonded at a distance of ∼3.4 Å. However, at 21 MPM when no trace of hydrogen bonding remains, the first-shell N−N peak narrows and becomes more symmetric: the asymmetry of the N−N correlation is therefore a signature of hydrogen bonding.

Integration of peaks 1 and 2 of the Gaussian fit to $r^2 g_{XX}(r)$ (Figure 7) yields first-shell coordination numbers on the order of ∼12, ∼8, and ∼6 molecules around a central nitrogen for 0, 8, and 21 MPM solutions, respectively. The equivalent integration in r space of peaks 2−4 of the Gaussian fit to $r^2 g_{XH}(r)$ (Figure 6) gives the corresponding number of second-shell hydrogen atoms surrounding a central nitrogen atom as 34, 25, and 19, corresponding to ∼11, ∼8, and ∼6 molecules around the nitrogen atom for 0, 8, and 21 MPM solutions. However, the coordination numbers of the X−X and X−H peaks in the

Table 2. Peak Assignments and Coordination Numbers: H−H Correlations

H−H assignment	0 MPM		8 MPM		21 MPM	
	r/Å	area/atoms	r/Å	area/atoms	r/Å	area/atoms
intra-H−H	1.64 ± 0.02	2.2 ± 0.2	1.64 ± 0.02	2.2 ± 0.2	1.64 ± 0.02	2.2 ± 0.2
inter-H−H	2.82 ± 0.05	7.5 ± 1.0	2.87 ± 0.06	5.0 ± 1.0	3.00 ± 0.07	3.0 ± 1.0
inter-H−H	4.14 ± 0.29	28 ± 2	4.21 ± 0.35	22 ± 2	4.38 ± 0.36	21 ± 2
inter-H−H	5.31 ± 0.20	23 ± 2	5.34 ± 0.23	16 ± 2	5.60 ± 0.25	18 ± 2

Table 3. Peak Assignments and Coordination Numbers: X−H Correlations

X−H assignment	0 MPM		8 MPM		21 MPM	
	r/Å	area/atoms	r/Å	area/atoms	r/Å	area/atoms
intra-N−H	1.03 ± 0.01	3.1 ± 0.2	1.03 ± 0.01	2.8 ± 0.2	1.03 ± 0.01	3.0 ± 0.2
inter-N−H (H-bonded)	2.42 ± 0.02	2.1 ± 0.3	2.45 ± 0.05	0.7 ± 0.2		0.0
inter-N−H	3.40 ± 0.08	11 ± 1	3.36 ± 0.10	6 ± 1	3.34 ± 0.10	3.0 ± 0.5
inter-N−H	4.17 ± 0.08	21 ± 2	4.14 ± 0.09	18 ± 1	4.12 ± 0.10	16 ± 2
inter-N−H	5.10 ± 0.15	12 ± 2	5.19 ± 0.12	10 ± 2	5.20 ± 0.15	10 ± 2

Table 4. Peak Assignments and Coordination Numbers: X−X Correlations

X−X assignment	0 MPM		8 MPM		21 MPM	
	r/Å	area/atoms	r/Å	area/atoms	r/Å	area/atoms
inter-N−N	3.59 ± 0.05	8.5 ± 0.5	3.52 ± 0.07	5.6 ± 0.5	3.49 ± 0.05	4.1 ± 0.5
inter-N−N	4.40 ± 0.12	4.0 ± 0.6	4.20 ± 0.10	2.9 ± 0.5	4.27 ± 0.6	1.8 ± 0.4
inter-N−N	5.10 ± 0.12	4.0 ± 1.0	4.88 ± 0.14	2.8 ± 0.5	4.82 ± 0.11	2.1 ± 0.4

21 MPM solution, obtained by integrating to ∼4.0 and 4.8 Å, respectively, are greater than those expected for an isolated tetrahedron of ammonia molecules around a cation. This suggests the presence of a second shell of solvent molecules surrounding the lithium ion.

B. Cation Solvation and Cation−Cation Structure. Previous studies have shown that lithium is strongly tetrahedrally solvated by ammonia, with an average first-shell Li−N distance of ∼2 Å.[16,17] Via RMC modeling,[19] we are now able to produce a detailed picture of the second solvation shell of ammonia molecules around the lithium cation, which takes into account the angular dependence relative to the primary tetrahedral solvation shell, as well as the distance from the cation. Figure 8 shows the RMC fit to the three total structure factors, while a comparison between the RMC and measured partial pair correlation functions is given in Figure 9. Analysis of the relative orientation of the ammonia molecules in the first and second solvation shells was carried out with respect to a central Li−(NH$_3$)$_4$ unit, which was oriented so that one of the Li−N bonds lies along the z axis, and one N−Li−N angle lies in the xz plane.

By applying the same set of translation and rotation matrixes to the next nearest nitrogen atoms, we can build up a picture of the second shell's orientation relative to the first shell. In this way, we find a preference for the solvent molecules to lie above the faces and edges of the primary-shell tetrahedron. Simple geometric considerations then give a first-shell to second-shell N−N distance of 3.6 Å. This arrangement is in accordance with the second shell inferred from previous lithium-centered neutron experiments,[17] which predicted a second-shell $r_{Li-N} \approx 4$ Å. Indeed, the first peak in the current X−X pair correlation function, assigned to N−N correlations, extends further than this distance. The total coordination number for this feature is ∼6 atoms, which is greater than the 3 atoms that may be expected for an isolated single-shell tetrahedron. This is clear evidence of a second solvation shell, in which the N−N peak

comprises the three surrounding nitrogen atoms in the primary tetrahedral shell, plus nitrogen atoms above the three nearest faces or edges of the first shell.

Further evidence of this arrangement of Li−(NH$_3$)$_4$ species is present in the X−H pair correlation function (Figures 3 and 6). At saturation, the total number of hydrogen atoms around a nitrogen atom (intermolecular) is ∼19 (up to a distance of ∼5 Å), as may be expected given the likelihood of three nitrogen atoms around any nitrogen atom in the first shell, and a further three in the second shell. As the metal content is increased to saturation, the emergence of a second peak at ∼4.1 Å (Figure 3) is largely due to the fact that, at saturation, there will be few, if any, solvent molecules not bound to a cation. Any second shell must therefore be formed by ammonia molecules shared between two cations.[17] The solvent molecules' orientations are governed by the nearest cation at ∼2 Å distance, so the hydrogen atoms, rather than the nitrogen atoms, on the second-shell solvent molecules must point toward their next nearest lithium ion.

In the 8 MPM solution, a number of unbound ammonia molecules remain. The second shell is then likely to consist of some unbound and some cation-bound ammonia molecules. The coordination numbers for N−N and N−H intermolecular correlations are also higher, showing that a greater degree of packing is possible, despite the fact that the nearest-neighbor X−H distances show no decrease as the metal content is increased.
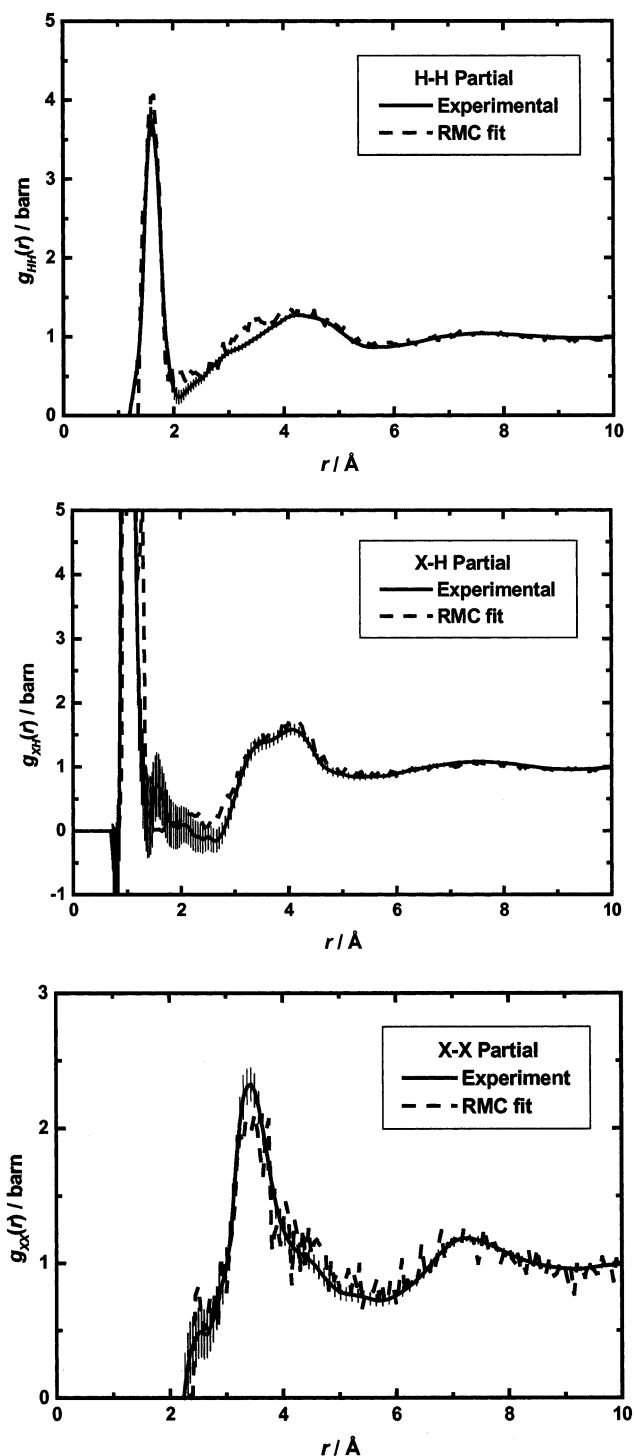
Armed with this picture of the cation solvation, we can turn our attention to the origin of the intermediate-range order that is observed in these solutions. At saturation, the first sharp diffraction peak in the total structure factor occurs at 1.00(2) Å^{-1}. This feature survives in all three of the composite partial structure factors. We therefore conclude that this signature of intermediate-range order must be caused by correlations between the host ammonia molecules, extending out to a distance of
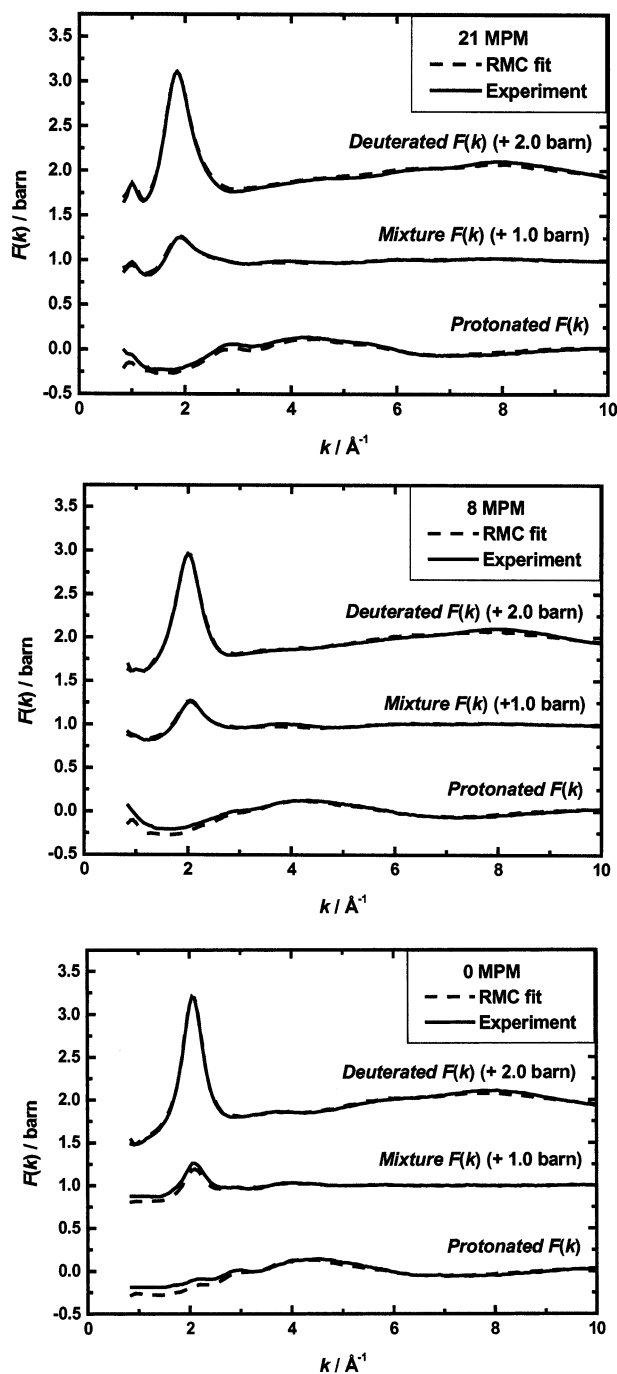
Figure 8. Reverse Monte Carlo fit to measured total structure factors: top curve, deuterated sample; middle curve, mixture sample; bottom curve, protonated sample.

Figure 9. Comparison between the RMC model and the measured partial pair correlation functions for the 21 MPM solution: solid line, experiment; dotted line, RMC model.

$\sim 2\pi/k = 6.3$ Å and with a coherence length defined by the prepeak width, Δk, and extending to $2\pi/\Delta k \approx 25$ Å. The prepeak position is consistent with contacts between solvated cations. Indeed, in lithium−methylamine solutions the corresponding prepeak shifts to a lower k value of 0.88(2) Å^{-1}, due to the increased solvated cation radius.[14,15]

C. Cavity Formation. One of the outstanding challenges of metal−ammonia solutions is to understand their fascinating electronic properties in terms of their microscopic structure.[12,13] In this context, a great deal of relevant information has already been collected, particularly from magnetic resonance measurements, X-ray diffraction, and ab initio simulations.[3,7−13,16] For

example, it has been postulated that an isolated excess electron occupies a solvent cavity of approximate radius 3 Å. However, we know very little about the snapshot structure of such polaronic voids, channels, or low-density regions through which the solvated electrons might percolate. Ideally, therefore, we would like to generate an excess-electron-centered view of our solutions, much as we have just done for H, N, and Li. The problem, of course, is that in terms of neutron scattering this amounts to looking for "the dog that did not bark".[27] We have
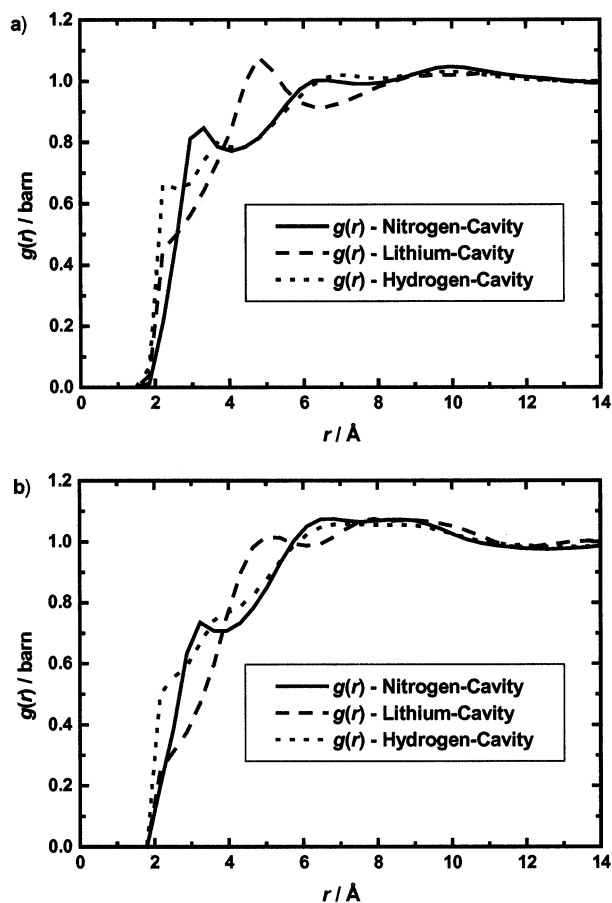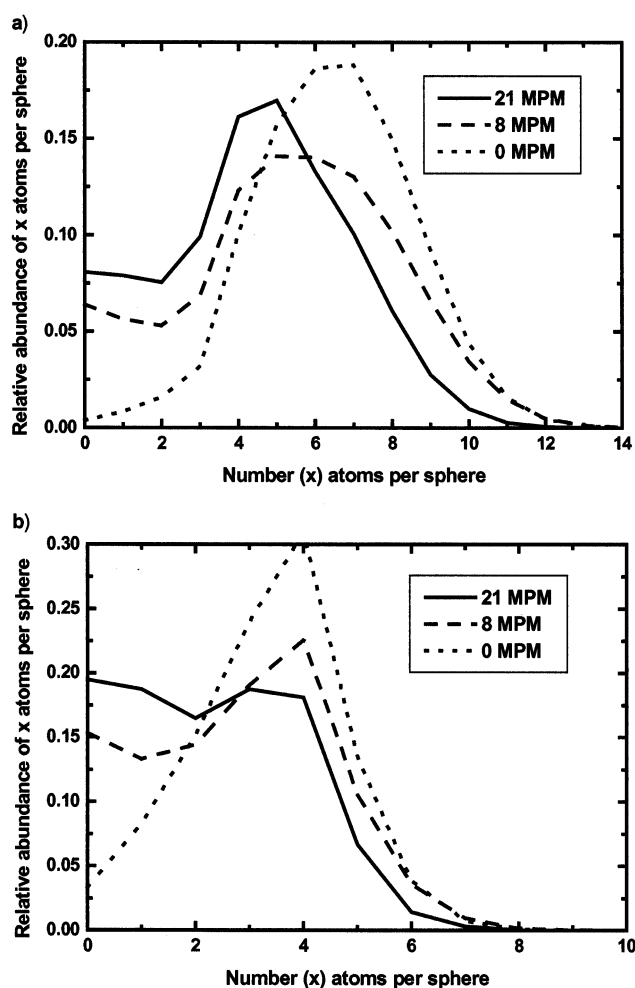
Figure 10. Nitrogen−cavity, lithium−cavity, and hydrogen−cavity pair correlation functions in the (a) 21 MPM solution and (b) 8 MPM solution. The sharp cutoff for the hydrogen−cavity function arises because the cavity is strictly defined as a sphere containing zero atomic centers, and the hydrogen atoms reside closest to these spherical voids.

therefore generated a 3-dimensional RMC[19] model that is constrained by our data, and have subsequently analyzed the molecular configurations for potential solvent cavities.

Analysis of the propensity and relative positioning of cavities within the RMC model was carried out in the following way: points were chosen approximately every 0.2 Å in the *x*, *y*, and *z* directions, and a sphere of radius 2.5 Å was defined around that point. A minimum image convention was applied to the cubic box, and the number of atom centers (lithium, nitrogen, or hydrogen) lying within each sphere was recorded. One might argue that this definition of a cavity (that is, no atomic *centers* lying within the sphere) leads to an overestimation of the cavity radius, since the atomic sizes have not been taken into account. However, by calculating the nitrogen−cavity, hydrogen−cavity, and lithium−cavity pair correlation functions, shown in Figure 10, we are able to estimate the number of atoms, hence an "atomic volume", that encroach on the spherical void. Upon integrating the radial distribution functions to a distance equal to the sum of the cavity radius and the atomic radius, we find a very low coordination number of ∼4.8 and ∼5.6 atoms for 21 and 8 MPM solutions, respectively. The maximum atomic volume as defined above is less than 3% of the spherical cavity volume, for both the 8 and 21 MPM solutions, so the method of cavity analysis used here is valid.
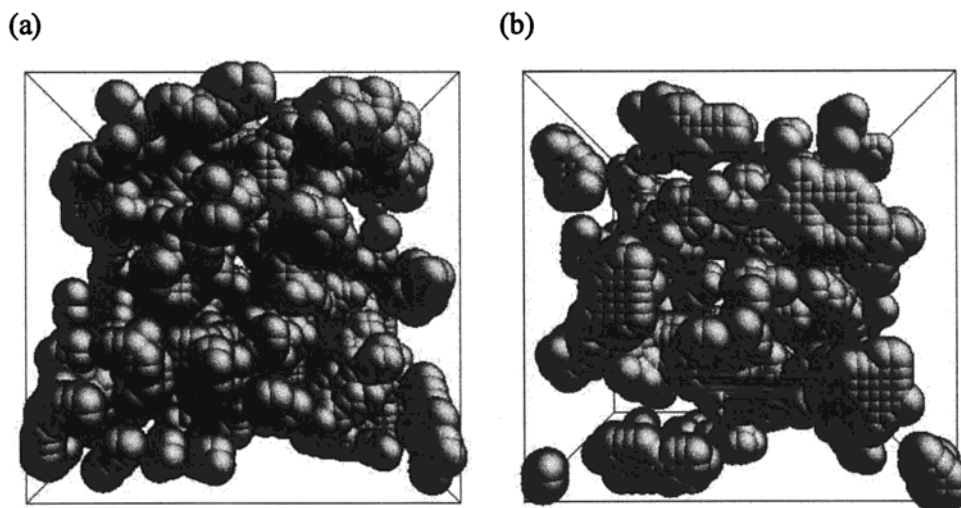
(27) Conan Doyle, A. *The memoirs of Sherlock Holmes: "Silver Blaze"*; Strand Magazine, London, UK, 1892.

Figure 11. Probability of a sphere of (a) radius 2.5 Å and (b) radius 2.0 Å containing *x* number of atoms: comparison among 0, 8, and 21 MPM solutions. Note the significant difference in the probability of finding a sphere of zero or one atom in the metallic 8 and 21 MPM solutions as compared to the pure ammonia solvent.

The graphs in Figure 11 show the results of the analysis, and give credence to our initial hypothesis. In pure ammonia, there are very few regions of low solvent density; the most likely number of atoms per sphere of radius 2.5 Å is 7 (density considerations predict this number to be 6.5), and the distribution is symmetrical about its center. However, for 8 and 21 MPM the probability distribution shows the presence of a significant number of spheres containing zero or one atom, demonstrating that there are regions of lower atomic density throughout the solutions. Figure 12 shows the cavity distribution and their tendency to form channels in the 8 and 21 MPM solutions.

V. Conclusions

The technique of hydrogen/deuterium substitution in neutron diffraction has been used to extract detailed information concerning the nature of the solvent structure in pure ammonia and lithium−ammonia metallic solutions. We assert that the introduction of alkali metal to the ammonia solvent causes a significant disruption to the degree of hydrogen bonding present, from ∼2.0 hydrogen bonds per nitrogen atom in the ammonia solvent to 0.7 and 0.0 hydrogen bonds in 8 and 21 MPM solutions, respectively. In conjunction with a reverse Monte Carlo molecular modeling technique, we then build up a picture

Figure 12. Distribution of cavities throughout the (a) 21 MPM and (b) 8 MPM metallic solutions of lithium in ammonia. The shaded areas represent spheres containing zero nitrogen, hydrogen, or lithium atoms/ions.

of the intermolecular arrangement of solvent molecules around the cations. At saturation, a secondary solvation shell composed of ammonia molecules shared between two cations is apparent, in which the solvent molecules preferentially reside above the faces and edges of the primary tetrahedral solvation shell. Such a packing arrangement will naturally give rise to the observed intermediate-range order, over a length scale of about 6−7 Å corresponding to the mean distance between solvated cations. Contrary to a large density decrease occurring upon addition of alkali metal to ammonia, we note a shift *inward* of the nearest-neighbor N−N distance. This observation, in addition to the 6-fold coordination of the first N−N peak, immediately suggests that the density decrease is caused by formation of cavities/channels between the solvated cation species. Analysis of the 3-dimensional model obtained via RMC further supports

this hypothesis. Indeed, nanosegregation of regions of lower and higher atomic density is clearly observed, to allow percolation of the dissociated (excess) electrons, leading to the formation of the highly conducting metallic state.

JA021227S